MSDE

PAPER

View Article Online
View Journal | View Issue

Cite this: *Mol. Syst. Des. Eng.*, 2025, **10**, 567

Bioinspired design rules for flipping across the lipid bilayer from systematic simulations of membrane protein segments†

ByungUk Park [a] and Reid C. Van Lehn *[ab]

The orientation of integral membrane proteins (IMPs) with respect to the membrane is established during protein synthesis and insertion into the membrane. After synthesis, IMP orientation is thought to be fixed due to the thermodynamic barrier for "flipping" protein loops or helices across the hydrophobic core of the membrane in a process analogous to lipid flip-flop. A notable exception is EmrE, a homodimeric IMP with an N-terminal transmembrane helix that can flip across the membrane until flipping is arrested upon dimerization. Understanding the features of the EmrE sequence that permit this unusual flipping behavior would be valuable for guiding the design of synthetic materials capable of translocating or flipping charged groups across lipid membranes. To elucidate the molecular mechanisms underlying flipping in EmrE and derive bioinspired design rules, we employ atomistic molecular dynamics simulations and enhanced sampling techniques to systematically investigate the flipping of truncated segments of EmrE. Our results demonstrate that a membrane-exposed charged glutamate residue at the center of the N-terminal helix lowers the energetic barrier for flipping (from ~12.1 kcal mol^{-1} to ~5.4 kcal mol^{-1}) by stabilizing water defects and minimizing membrane perturbation. Comparative analysis reveals that the marginal hydrophobicity of this helix, rather than the marginal hydrophilicity of its loop, is the key determinant of flipping propensity. Our results further indicate that interhelical hydrogen bonding upon dimerization inhibits flipping. These findings establish several bioinspired design principles to govern flipping in related materials: (1) marginally hydrophobic helices with membrane-exposed charged groups promote flipping, (2) modulating protonation states of membrane-exposed groups tunes flipping efficiency, and (3) interhelical hydrogen bonding can be leveraged to arrest flipping. These insights provide a foundation for engineering synthetic peptides, engineered proteins, and biomimetic nanomaterials with controlled flipping or translocation behavior for applications in intracellular drug delivery and membrane protein design.

Received 26th February 2025,
Accepted 6th May 2025

DOI: 10.1039/d5me00032g

rsc.li/molecular-engineering

Design, System, Application

We present a bioinspired design strategy for engineering membrane proteins or related materials with the ability to "flip" polar or charged groups across the hydrophobic core of the cell membrane in a process similar to lipid flip-flop. Drawing inspiration from the behavior of EmrE, an integral membrane protein which has an N-terminal helix known to flip across the membrane, we use molecular simulations to systematically study the flipping of segments of the EmrE sequence. By comparing corresponding flipping thermodynamics, we develop bioinspired design rules for tuning the chemical features of membrane-exposed and solvent-exposed groups to promote flipping. Our analysis reveals that a membrane-exposed group plays a critical role in controlling flipping by stabilizing water defects in the membrane to reduce flipping energy barriers. Comparative analysis highlights the N-terminal helix's unique susceptibility to flipping due to charge-induced membrane perturbations as well as the role of hydrogen bonding between membrane-exposed groups to inhibit flipping. Based on these sequence features, we establish molecular-scale design rules for tuning the local chemical environment to control flipping, which will be valuable for applications such as drug delivery or signaling in which synthetic materials must bypass the lipid membrane to access intracellular environments.

1. Introduction

The cell membrane is the boundary between the interior of a cell and the exterior environment and plays a critical role in regulating transport into and out of the cell. The membrane primarily consists of a phospholipid bilayer whose hydrophobic core prevents the unregulated diffusion of

[a] *Department of Chemical and Biological Engineering, University of Wisconsin –Madison, Madison, Wisconsin 53706, USA. E-mail: vanlehn@wisc.edu*
[b] *Department of Chemistry, University of Wisconsin–Madison, Madison, Wisconsin 53706, USA*

† Electronic supplementary information (ESI) available: Additional methodological details, detailed simulation protocols and analysis of convergence, additional analysis of hydrogen bonding, additional free energy calculations. See DOI: https://doi.org/10.1039/d5me00032g

charged molecules across the membrane. Instead, integral membrane proteins (IMPs) play essential roles in controlling transport, signaling, and enzymatic activity. IMPs have transmembrane α-helices (TMHs) that are embedded in the lipid bilayer and connected by water-exposed loops.[1] Most IMPs are inserted into the membrane during protein synthesis at which point their topologies (*i.e.*, orientations of structural elements relative to the membrane) are determined.[2,3] Currently, the prevailing view is that IMP topology remains fixed after insertion.[3,4] Recent studies, however, provide experimental evidence that single TMHs[5] and IMPs with multiple TMHs can undergo topological rearrangements after protein synthesis.[6–11] These rearrangements require the translocation of water-soluble (charged or polar) loops across the hydrophobic core of the lipid bilayer in a manner analogous to lipid flip-flop;[12] we refer to this behavior as "flipping". For example, pH-low insertion peptides[13,14] and single TMHs[5] have been experimentally observed to flip across single-component lipid membranes in response to a change in pH. The flipping of a hydrophilic loop is surprising because the translocation of polar, and particularly charged, species across the hydrophobic core of the lipid bilayer is associated with a high free energy barrier and corresponding long timescale.[15–17] Understanding the molecular details of these flipping pathways would be valuable for rationally designing membrane-permeating peptides or other synthetic materials as drug delivery agents.[16–20]

Flipping has also been observed for IMPs with multiple TMHs. Notably, EmrE is a well-known small multidrug resistance (SMR) transporter from *Escherichia coli* that effluxes positively charged polyaromatic substrates against the concentration gradient by coupling to proton transport, rendering bacteria resistant to a variety of toxic compounds.[21] EmrE is a homodimer consisting of two identical monomers, each with four TMHs, that insert into the membrane in two opposite orientations with equal probability; oppositely oriented monomers then assemble into a stable EmrE dimer (Fig. 1a).[10,22–24] Considering that other multidrug transporter protein superfamilies have 5–14 TMHs,[25] the capability of SMR proteins to facilitate the proton-coupled transport of a wide variety of substrates while having small sizes (~12 kDa) has motivated substantial research interest.[26–29] Due to its size, stability, and retention of its function upon solubilization in detergent, EmrE is a prototypical SMR protein that provides a unique experimental paradigm for biochemical and biophysical studies of such membrane based ion-coupled transporters.[21] Since dimerization requires two oppositely oriented monomers, EmrE's function depends on the topology of its

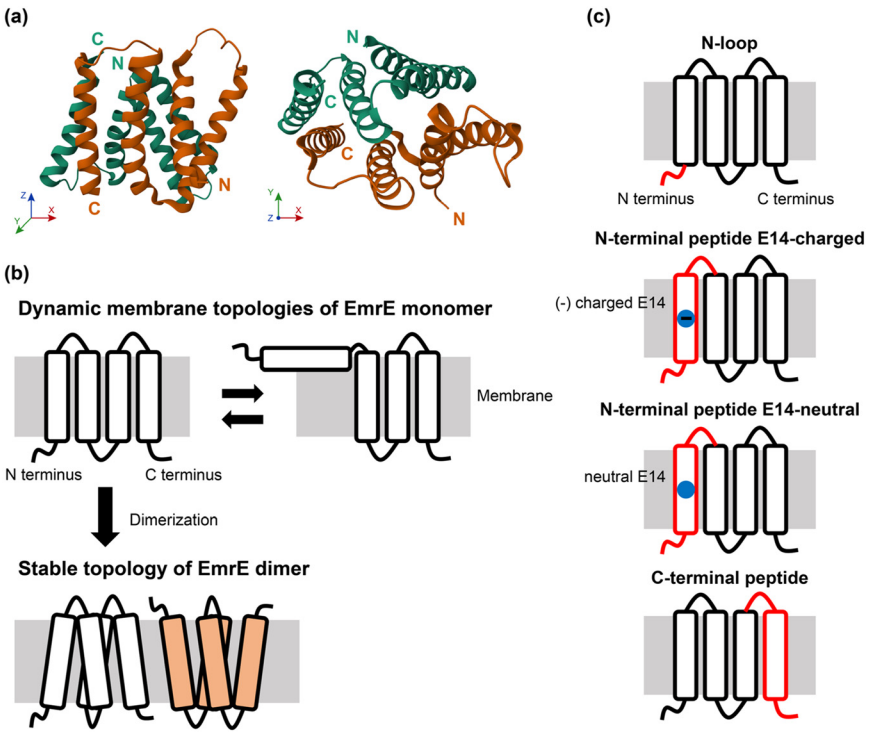

Fig. 1 Structure, topology, and sequence of EmrE and truncated segments studied in this work. (a) Structure of the EmrE dimer viewed from within the *x*–*y* plane of the membrane (left) or down the *z*-axis from above the membrane (right). The two monomers are colored green (chain A) and orange (chain B). The N- and C-termini for each monomer are labeled with "N" and "C", respectively. (b) Schematic of dynamic membrane topologies of the EmrE monomer,[32] in which the N-terminal (but not C-terminal) transmembrane helix crosses (flips) across the membrane (top). Flipping is no longer observed experimentally after the monomers assemble into a dimer (bottom). (c) Schematics of the truncated segments (colored in red) from the EmrE monomer that are used for the simulations in this work. The blue dot indicates the approximate position relative to the membrane of the E14 residue. Corresponding amino-acid sequences are shown in Fig. 2–4.

monomers. Interestingly, EmrE monomers can undergo topological rearrangements involving the reorientation of loops and TMHs (*i.e.* flipping) after initial membrane insertion, which is thought to promote dimerization.[8–10,30] While the reorientation of the complete EmrE monomer is likely very slow (as it has been observed experimentally on a >20 minute timescale),[31] the reversible flipping of the N-terminal TMH and its loop has been observed on a biologically relevant ~minute timescale for a single EmrE monomer.[32] An even more dramatic topological rearrangement has been experimentally observed in LacY, a 12-TMH symporter. In LacY, six of the 12 TMHs can flip across the membrane on comparable timescales in response to changes in the ratio of lipids with zwitterionic phosphatidylethanolamine (PE) or anionic phosphatidylglycerol (PG) head groups in the surrounding membrane.[6,33] Remarkably, this rearrangement occurs even in lipid vesicles lacking any potential chaperones.[34] These observations suggest that flipping may involve the direct translocation of loops and TMHs within complete IMPs across the bilayer, and as such can provide insights to inform the design of macromolecules or larger biomaterials capable of crossing lipid membranes.

Experimentally resolving the molecular-scale mechanisms underlying flipping is challenging. Alternatively, molecular simulations coupled with enhanced sampling methods have been used in a variety of systems (*e.g.*, small molecules, nanoparticles, peptides, proteins) to model their interactions with or translocation across lipid bilayers.[35–39] For example, past simulation studies have estimated that the free energy barrier for the translocation of simple ions across the lipid bilayer is ~25 kcal mol^{-1},[15] which is consistent with a corresponding hour-day translocation timescale. Numerous simulations have shown that this free energy barrier is due to the formation of a local water defect that permits the solvation of the translocating species but perturbs bilayer structure.[40–43] However, the free energy cost for this perturbation is sensitive to other species in the local chemical environment. For example, membrane-exposed charged residues on TMHs can stabilize water defects, thereby reducing the free energy barrier associated with ion translocation or the flipping of hydrophilic peptide loops.[38,39,44] Charge-induced defect formation was also observed during the translocation of cell-penetrating peptides.[16,17] Protonation state plays a role in this effect, as neutral membrane-exposed residues do not reduce the barrier to the same extent as charged residues.[38,39] The translocation of multiple charged residues across the membrane similarly is not additive because the cost for translocation of a second residue is decreased due to the stabilization of a water defect by the first residue.[45,46] The overall protein content of the membrane can reduce translocation barriers through bilayer disruption or stabilizing intermediate states during translocation.[47,48] Similar barriers have been reported for the flipping of lipids and other amphiphiles depending upon the length of the amphiphile's nonpolar group.[35,37,49] These findings highlight how the local chemical environment strongly impacts the flipping of polar and charged groups, motivating further study of sequence features that affect TMH flipping.

EmrE (Fig. 1a) serves as an ideal template for the study of TMH flipping because a recent study by Seurig *et al.* provided experimental insight into several factors that influence its topological rearrangements.[32] Key experimental observations (Fig. 1b) include: (1) the N-terminal TMH1 and its loop can flip across the bilayer on a timescale of minutes, (2) the C-terminal TMH4 is not observed to flip, and (3) flipping is only observed for the EmrE monomer and is arrested upon dimerization. The timescale for TMH1 flipping is surprisingly short when compared to the reported hour-day time scale associated with the simple diffusion of charged ions across lipid bilayers, even though flipping requires a hydrophilic loop to cross the bilayer.[15] This behavior of EmrE may be attributed to an unusual pattern in the EmrE TMH1 sequence compared to other TMHs in the *Escherichia coli* inner-membrane proteome. According to comprehensive analyses of amino-acid sequences of experimentally characterized IMPs, most have a relatively high number of charged residues in their solvent-exposed loops with nonpolar residues in their TMH domains.[50,51] In contrast, the EmrE sequence contains nonpolar residues in its short N-terminal loop and a relatively high number of charged residues in TMH1, thus conferring marginal hydrophilicity to the N-terminal loop and marginal hydrophobicity to TMH1 (Fig. S1†).[30] These sequence differences for the EmrE helices may contribute to their experimentally observed flipping behavior and, thus, characterizing the flipping of EmrE termini may provide insights into fundamental factors encoded in the sequence that enhance translocation across the membrane.

In this work, we use all-atom molecular dynamics (MD) simulations to investigate mechanisms underlying the flipping of peptides whose sequences mimic different sets of functional domains of EmrE. We systematically model the flipping of truncated segments of EmrE as representative analogues of its N- or C-terminal TMHs, as well as the N-terminal loop, to identify the impact of helix and loop properties on flipping free energy barriers. Using replica-exchange umbrella sampling simulations, we find that the barrier for the flipping of the N-terminal TMH is substantially lower than the barrier for the translocation of the isolated N-terminal loop, indicating that the presence of the TMH is important to flipping behavior. Comparison of the N-terminal helix with a charged membrane-exposed glutamate (E14) residue, neutral E14 residue, and the C-terminal helix indicates that the charged E14 residue permits this small flipping free energy barrier. We further simulate N- and C-terminal flipping in the complete EmrE monomer to show that the same trends identified for truncated segments are preserved but with higher free energy

barriers due in part to hydrogen-bonding between TMHs. Additional simulation of the EmrE dimer suggests that substantial hydrogen bonding between TMH1 and other helices upon dimerization likely arrests flipping. Together, these results provide mechanistic and thermodynamic insight into sequence features that affect the flipping of TMHs inspired by EmrE to provide insight into design rules for synthetic materials capable of translocating charged elements across cellular membranes.

2. Methods

2.1. Structures and force fields for truncated segments, protein, and lipids

The EmrE structure with PDB ID 7JK8 (ref. 52) and 110 amino-acid residues was used as the template 3D structure for all performed simulations and analysis. EmrE chain B was chosen for the monomer system since subunit B is experimentally observed to be more dynamic when embedded inside the lipid bilayer.[52] The sequence of the truncated C-terminal peptide (C-pep) encompassed the first residue of the fourth solvent-exposed loop to the C-terminal residue (residues 79–110; illustrated in Fig. 1c). The truncated N-terminal peptide encompassed the N-terminal residue to the last residue of the second solvent-exposed loop (residues 1–31). The truncated N-terminal peptide was modeled in two sets of simulations: one with a neutral, protonated E14 (N-pep-neut) and one with a charged, deprotonated E14 (N-pep-charge). The truncated N-terminal loop (N-loop) encompassed only the first N-terminal loop that is exposed to the solvent when EmrE is in its stable membrane topology (residues 1–4). The EmrE monomer systems encompassed the complete sequence of 110 residues with a charged E14 residue.

A single-component 1,2-dimyristoyl-*sn*-glycero-3-phosphocholine (DMPC) lipid bilayer was used to represent the lipid membrane. DMPC has been widely used as a model membrane for previous MD simulation studies on EmrE[52,53] and the chosen EmrE structure was experimentally determined by solid-state NMR of the EmrE dimer in DMPC bilayers.[52] Using a single-component lipid bilayer also removes any contributions from different lipid components to the flipping processes, thereby highlighting only sequence-encoded characteristics that contribute to the flipping of EmrE segments. 100 and 99 lipids were added to each bilayer leaflet (199 lipids total) for the EmrE monomer system (Fig. S2†), 80 lipids were added to each bilayer leaflet (160 lipids total) for the truncated peptide systems, and 40 lipids were added to each bilayer leaflet (80 lipids total) for the N-loop system. The thickness of the surrounding water layer was set to 4.5 nm, which was sufficient to model fully hydrated lipid bilayers and avoid self-interactions due to periodic boundary conditions. All systems were modeled using the CHARMM36m force field[54–56] with WYF parameters for cation–π interactions and the TIP3P water model. Molecular structures and force field parameters for the peptides and lipid bilayer were generated using the CHARMM-GUI Input Generator.[57–60] Acetyl and amide groups were added to cap the N- and C-termini of all peptides and the proteins to permit apples-to-apples comparisons between these systems. The orientation of the inserted segments (and complete monomer) relative to the DMPC membranes were aligned with the experimentally characterized EmrE structure using the PPM server.[61] All systems were neutralized with 20 mM NaCl to match the experimental conditions of the previous solid-state NMR study.[52] The number of components of the systems simulated in this work are summarized in Table S1.†

2.2. Simulation protocol

Equilibration. All systems were energy-minimized using the steepest descent algorithm until the maximum force between atoms reached the criterion of <1000 kJ mol^{-1} nm^{-2}. After energy minimization, all systems were equilibrated at constant NVT for 250 ps then further equilibrated for 20 ns at constant NPT. The EmrE monomer system was equilibrated for an additional 500 ns (520 ns in total) at constant NPT. During equilibration, the temperature was maintained at 310.15 K using a Berendsen thermostat with a time constant of 1.0 ps and the pressure was maintained during NPT equilibration at 1 bar using a semi-isotropic Berendsen barostat with a time constant of 5.0 ps and a compressibility of 4.5×10^{-5} bar^{-1}.[62] All MD simulations were performed using a leapfrog integrator with a 2 fs timestep using Gromacs 2021.[63] Verlet lists were generated using a 1.2 nm neighbor list cutoff, van der Waals interactions were modeled with a Lennard-Jones potential using a 1.2 nm cutoff that was smoothly shifted to zero between 1.0 and 1.2 nm, and electrostatic interactions were calculated using the smooth particle-mesh Ewald method with a short-range cutoff of 1.2 nm, a grid spacing of 0.14 nm, and fourth-order interpolation.[64] Bonds with hydrogen atoms were constrained using the LINCS algorithm.[65]

Steered molecular dynamics. To generate initial configurations for umbrella sampling, steered MD (SMD) was performed to pull loops for each of the N-pep-neut, N-pep-charge, C-pep, N-loop, and EmrE monomer systems from their equilibrated locations in aqueous solution across the bilayer. Pulling was performed by applying a harmonic biasing potential using the cylindrical pull coordinate geometry implemented in Gromacs with a 0.0005 nm ps^{-1} pulling rate and 1000 kJ mol^{-1} nm^{-2} force constant. The *z*-component of the distance between the center-of-mass (COM) of the bilayer and the COM of the pulled loop, *dz*, was used as the reaction coordinate for both steered MD and umbrella sampling (*vide infra*). By using the cylindrical pull coordinate geometry, only the portion of the bilayer within a cylindrical region around the pulled loop was used when computing the COM of the bilayer, which is accomplished by weighting the contribution of each atom

to the calculation of the reaction coordinate by a factor w_i which is defined in eqn (1):

$$w_i = \begin{cases} 1 - 2\left(\frac{r_i}{r_{\text{cyl}}}\right)^2 + \left(\frac{r_i}{r_{\text{cyl}}}\right)^4, & r_i < r_{\text{cyl}} \\ 0, & r_i \leq r_{\text{cyl}} \end{cases} \quad (1)$$

Here, r_i is the radial distance between atom i and the COM of the pulled loop in the x–y plane and r_{cyl} = 1.5 nm for all SMD and umbrella sampling simulations. Position restraints were applied to the z-component of the positions of the phosphorus atoms of the DMPC lipids with a harmonic constant of 1000 kJ mol^{-1} nm^{-2} to avoid unphysical lipid fluctuations or the creation of large bilayer defects during steered MD.

Since pulling a loop across the bilayer in a single direction might introduce an orientational bias when using initial configurations taken from SMD simulations during umbrella sampling (Fig. S3†), and thus potentially hysteresis in the resulting free energy profiles[44] (as demonstrated in Fig. S4†), SMD simulations were performed following a two-stage protocol in which loops were pulled across the bilayer in both directions. First, the loops of the N-pep-neut, N-pep-charge, C-pep, and EmrE monomer were pulled for 5.5 nm across the bilayer from their initial configurations to ensure the complete flipping of the pulled loop across the bilayer, while the N-loop was pulled for 6 nm from one side of the bilayer to the other. After this first pulling step, additional NPT equilibration was performed for 5 ns using the same parameters as initial system equilibration. During equilibration, the previously applied position restraints on the lipid phosphorus atoms were removed while the harmonic bias was applied to the z-component of the distance between the COM of the bilayer and the COM of the pulled loop to avoid any deviation of their relative positions. The second stage of SMD was then performed by using the same pull parameters from the first stage of SMD except with the opposite sign of the pull direction, thereby pulling the loop in the opposite direction across the bilayer. Initial configurations from both pulling trajectories were then used to initiate umbrella sampling as described below.

Replica exchange umbrella sampling. Replica exchange umbrella sampling (REUS), also referred to as Hamiltonian replica exchange MD,[66] window-exchange umbrella sampling,[67,68] or bias-exchange umbrella sampling,[69] was performed to compute potentials of mean force (PMFs) for the flipping of different types of truncated EmrE segments and loops of EmrE monomer across the DMPC bilayer. The temperature was maintained at 310.15 K using a Nosé–Hoover thermostat with a time constant of 1.0 ps and the pressure was maintained at 1 bar using a semi-isotropic Parrinello–Rahman barostat with a time constant of 5.0 ps and a compressibility of 4.5 × 10^{-5} bar^{-1}. Umbrella sampling was performed using 56–61 windows spaced by 0.1 nm along the reaction coordinate, which was defined as the z-component of the distance between the COM of the bilayer and the COM of the pulled loop computed using the cylindrical pull coordinate geometry (defined in the previous section). Initial configurations for the windows were selected from the two SMD trajectories that led to pulling across the bilayer in opposite directions, with configurations from sequential windows taken from alternating SMD trajectories (*i.e.*, windows 1, 3, 5, … used initial configurations from one SMD trajectory while windows 2, 4, 6, … used initial configurations from the other SMD trajectory). This approach helped eliminate bias associated with the orientation of the pulled loop during its initial pulling across the bilayer, as discussed in the ESI† (Fig. S3 and S4). For the EmrE monomer, windows 0 to 18 used initial configurations exclusively from the first SMD trajectory because the second SMD trajectory in the opposite direction was unable to sample configurations from these windows due to steric hindrance between the pulled loop and rest of the monomer. All windows were simulated by applying a 1000 kJ mol^{-1} nm^{-2} harmonic constant to sample the chosen value of the reaction coordinate. Each window was initially equilibrated without replica exchange for 1 ns at constant NPT, then each window for the C-pep and N-pep-neut peptides was simulated for 200 ns while each window for the N-pep-charge, N-loop, and EmrE monomer was simulated for 100 ns. These simulation times were determined based on the convergence of the resulting PMF curves (Fig. S7–S12†). Replica exchange between adjacent windows was attempted with a time interval of 10 ps (Fig. S5 and S6†).[70,71] The initial 10 to 60 ns of the REUS trajectories were discarded as equilibration depending on the system and convergence analysis (Fig. S7–S12†), and the rest of the trajectories were used to compute PMFs using the Weighted Histogram Analysis Method (WHAM) with error estimated using bootstrapping.[72] WHAM was performed using 200 bins along the reaction coordinate and bootstrapping was performed 200 times using the given histograms with the integrated autocorrelation time, t, estimated for each umbrella window and then used as a weight for the respective window with $1/(1 + 2t/\mathrm{d}t)$. Complete simulation details are presented in the ESI.†

Unbiased simulations of EmrE monomer and dimer. Unbiased MD simulations of the EmrE monomer and dimer systems were performed for analysis of hydrogen bonds (H-bonds). The system setup for the monomer is described above; the dimer used the same approach for consistency in system preparation but with 200 and 203 lipids added to each bilayer leaflet (403 lipids total) due to the larger area occupied by the dimer (Fig. S2†). The same MD and force field parameters were also used for the equilibration of these systems. For NPT production simulations, the temperature was maintained at 310.15 K using Berendsen thermostat with a time constant of 1.0 ps and the pressure was maintained at 1 bar using a semi-isotropic Berendsen barostat with a time constant of 5.0 ps and a compressibility of 4.5 × 10^{-5} bar^{-1}. Both the monomer and dimer systems were simulated for 500 ns and system configurations were extracted every 10 ps during the NPT production simulations.

2.3. Analysis

The time-averaged densities of water molecules and phosphorous atoms of the DMPC lipid headgroups were calculated using MDTraj (v.1.9.7).[73] Densities were computed from and averaged over the entire REUS trajectory per umbrella sampling window as a function of the z-component of the distance between the COM of the bilayer and the COM of the water/phosphorous atoms. Densities were then histogrammed based upon the z-component value in a range from −4.0625 nm to 4.0625 nm by using 65 bins (bin width = 0.125 nm). The helicity was defined as the sum of the set of root-mean-squared distances (RMSDs) between a peptide configuration (R_i) and an idealized α-helical structure (R^0) according to eqn (2) and (3).[74]

$$\text{Helicity} = \sum_{\alpha} n\left[\text{RMSD}\left(\{R_i\}_{i\in\Omega_\alpha}, \{R^0\}\right)\right] \quad (2)$$

$$n(\text{RMSD}) = \frac{1-(\text{RMSD}/0.1)^8}{1-(\text{RMSD}/0.1)^{12}} \quad (3)$$

The sum runs over all possible segments of a helix (Ω_α) and measures the number of six-residue segments that have an α-helical configuration. The helicity was computed by post-processing trajectories using PLUMED (v.2.8.0)[75] and computing the ALPHARMSD CV (eqn (S4), Fig. S15†). H-bonds between TMHs of the complete EmrE monomer and dimer were characterized by using the Visual Molecular Dynamics (VMD) H-bond analysis tool.[76] Only the polar atoms N, S, O, F were selected for the analysis. The donor–acceptor distance cutoff was set to 3.5 Å and the angle cutoff was set to 30°. H-bonds for each system were computed using all the frames of the 500 ns unbiased trajectory.

3. Results and discussion

3.1. Flipping of the marginally hydrophilic N-terminal loop of EmrE

The overall goal of this study is to uncover design rules for sequence features that affect the flipping of TMHs with polar flanking loops by understanding mechanisms that promote the flipping of the N-terminal helix of the EmrE monomer. To do so, we sought to compare the free energy associated with the flipping of the truncated N-terminal helix to the free energy associated with flipping other truncated segments of EmrE to determine factors affecting flipping free energies. First, we modeled the free energy for the flipping of a truncated N-loop across the bilayer; this process could equivalently be called translocation since the N-loop is not embedded in the membrane. Due to its simple structure, comprising only four polar amino-acid residues (Fig. 2a), the PMF for the flipping of the N-loop is expected to be symmetric with respect to the bilayer since the lipid composition is identical in both leaflets and the configurations of the N-loop before and after flipping are effectively identical by symmetry, unlike the configurations of the truncated helices which have distinct configurations before and after flipping. Computing this PMF permits analysis of whether the simulation approach correctly yields a symmetric PMF and establishes a baseline free energy barrier for the flipping of a hydrophilic loop for comparison to flipping truncated helices. We then modeled the flipping of the N-terminal helix with a deprotonated E14 at the center of the helix and two flanking solvent-exposed loops (N-pep-charge) to compare the barrier height and PMF profile to that of the N-loop. Similar comparisons were made for the truncated C-terminal helix (C-pep) and truncated N-terminal helix with a protonated E14 (N-pep-neut), as described below.

Fig. 2a shows the PMF for N-loop flipping computed using the REUS approach described in the Methods. We performed REUS to calculate the PMF because hysteresis in the PMF was observed when using standard umbrella sampling with windows from either forward or backward steered molecular dynamics simulations, leading to an asymmetric PMF with respect to dz (Fig. S4†). Allowing the exchange of configurations between adjacent windows enhanced the convergence of the PMF calculations and eliminated hysteresis. The free energy barrier for flipping (ΔG_{flip}) was defined as the difference between the PMF maximum and PMF minimum and is the barrier that the N-loop (or truncated peptide when discussed below) must overcome during flipping. The N-loop PMF is approximately symmetric, as expected, with a maximum value near dz = 0 and with $\Delta G_{\text{flip}} \cong 7.5$ kcal mol^{-1} (Fig. 2a). This value of ΔG_{flip} is relatively small when compared to values of ΔG_{flip} computed for charged ions in previous MD simulation studies (≅25 kcal mol^{-1}),[15] which can be attributed to the short length of the N-loop and its inclusion of relatively hydrophobic residues (methionine, M, and tyrosine, Y).

Fig. 2b shows simulation snapshots of configurations at values of dz corresponding to notable features in the PMF. Snapshots (1) and (8) show two local PMF minima corresponding to positions where the N-loop is in solution near the bilayer-water interface, snapshots (2) and (7) show two local PMF maxima corresponding to positions where the N-loop crosses the bilayer head group region, and snapshots (3) and (6) show global PMF minima corresponding to positions where the N-loop is embedded in the bilayer head group region. As expected, configurations for the N-loop are similar when it interacts with the upper and lower leaflets of the bilayer, which is consistent with the symmetry of the PMF. Snapshots (4) and (5) show configurations near the PMF maximum. These snapshots illustrate the local deformation of the bilayer to facilitate solvation of the hydrophilic loop as it reaches the center of the bilayer. In addition, the orientation of the loop inverts between configuration (4) and (5), which is a consequence of the REUS protocol; this change in orientation is necessary to avoid an incorrectly asymmetric PMF[44] (Fig. S4†) and is a key benefit of the REUS methodology.

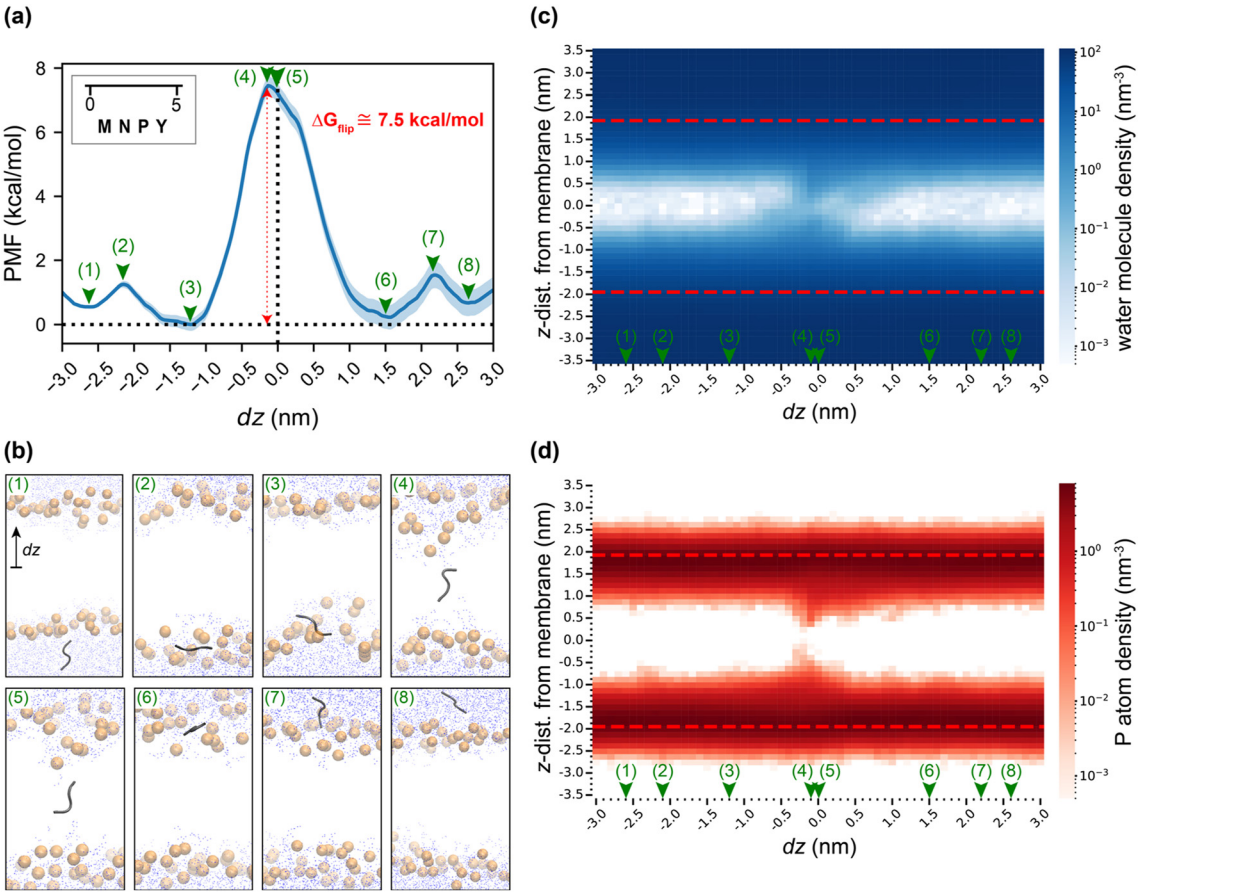

Fig. 2 Analysis of flipping for the truncated N-terminal loop (N-loop). (a) Potential of mean force (PMF) as a function of the *z*-component of the distance between the COM of the N-loop and the center of the membrane, *dz*. The amino-acid sequence of the N-loop is in the top-left inset. The midplane of the membrane is at *dz* = 0 nm. The blue shaded area indicates the standard deviation computed by bootstrapping. (b) Simulation snapshots of N-loop flipping. Each numbered snapshot corresponds to a representative configuration for the value of *dz* marked by a green arrowhead and corresponding number on the PMF curve in (a). The N-loop is gray, phosphorus atoms of lipid head groups are orange, water molecules are blue dots, and lipid tails are not shown to aid visualization. (c) Heatmap of water molecule number densities as a function of *dz*. Each point in the heatmap shows the density of water molecules with the specified *z*-component of the distance from the membrane midplane averaged over time and over all *x*–*y* positions. Densities are computed using configurations from the umbrella sampling trajectories with the value of *dz* (*i.e.*, the distance of the N-loop from the membrane midplane). The red dashed lines indicate the distances from the center of the membrane that correspond to the maximum average densities of phosphorus atoms from (d). (d) Heatmap of phosphorus atom number densities as a function of *dz*. Each point in the heatmap is computed as described for (c). Red dashed lines indicate the maximum average densities of phosphorus atoms.

Fig. 2c and d present analysis of membrane water content and bilayer structure to quantify the observed bilayer perturbation and explore the mechanistic origin of the PMF profile. Fig. 2c shows the average water density as a function of the *z*-component of the distance from the bilayer midplane computed from the REUS trajectories for different values of *dz*; the *y*-axis thus plots the distance used to compute water densities, while the *x*-axis indicates the distance of the N-loop from the membrane midplane. There is little variation in the water density for $dz < -1.0$ nm and $dz > 1.0$ nm since these values correspond to configurations in which the N-loop remains in solution or near the membrane head group region. For -1.0 nm $< dz < 1.0$ nm, a range in which the PMF increases as the N-loop crosses the hydrophobic core of the membrane, there is an increase in water density at regions close to the membrane midplane. These data are consistent with the water content visualized in snapshots (4) and (5) and indicates the formation of water defects that solvate the N-loop. Fig. 2d similarly quantifies the density of phosphorus atoms as a function of the same variables to indicate perturbations to the bilayer structure. Like the water density, there is an increase in intra-membrane phosphorus density for values of *dz* coinciding with the increase in the PMF. These results show that while small water defects were observed from the windows with the N-loop biased at the center of the membrane (Fig. 2b and c), no sizable membrane perturbation was captured from the same windows (Fig. 2d) due to the only marginal hydrophilicity of the N-loop.

3.2. Flipping of the marginally hydrophobic N-terminal helical domain of EmrE

Next, we tested how the addition of the marginally hydrophobic N-terminal TMH1 to the N-loop contributes to

both mechanistic and energetic differences in the flipping of the truncated N-terminal peptide. Fig. 3a shows the sequence of the truncated TMH1 and its two flanking loops. We first investigated the flipping of a truncated N-terminal peptide with a deprotonated (and hence charged) E14 residue, which we refer to as "N-pep-charge". Considering both the expected pK_a of E14 (ref. 77) and that E14 residues alternate their protonation states during the efflux of drug-like molecules,[52,78] we also compared this analysis to a peptide with protonated E14 residue ("N-pep-neut"), as described below, to investigate the role of the protonation state of the membrane-exposed residue on flipping. Since TMH domains in typical IMPs have compositions containing primarily hydrophobic residues,[79,80] EmrE's comparatively hydrophilic TMH1 due to the membrane-exposed E14 residue (Fig. S1†) was considered as one of the potential key factors that promotes the flipping of the N-terminal TMH1 when EmrE is in its monomer state.

Fig. 3b shows that the PMF profile for the flipping of the N-pep-charge peptide exhibits pronounced asymmetry compared to the N-loop (Fig. 2b). The global PMF minimum at $dz \approx -1.2$ nm corresponds to the peptide in a transmembrane state with its flanking loops exposed to solvent on either side of the bilayer. The corresponding snapshot (1) in Fig. 3c shows that at the PMF minimum water molecules enter the bilayer to solvate the charged E14 residue. Flipping then brings the N-loop from the lower leaflet ($dz < 0$) to the upper leaflet ($dz > 0$), with a maximum at $dz \approx 0.7$ nm. During this process, the N-terminal loop of the peptide crosses the bilayer while the helical segment mostly retains its initial orientation observed at the PMF global minimum. ΔG_{flip} of the N-pep-charge was ~5.4 kcal mol^{-1} which is smaller than ΔG_{flip} of the N-loop (7.5 kcal mol^{-1}). After the N-terminal loop crosses the bilayer ($dz > 0.7$ nm), the helical segment then flips across the bilayer while partial unfolding is observed, especially at G17 (shown visually in Fig. 3c and quantified based on changes to helicity

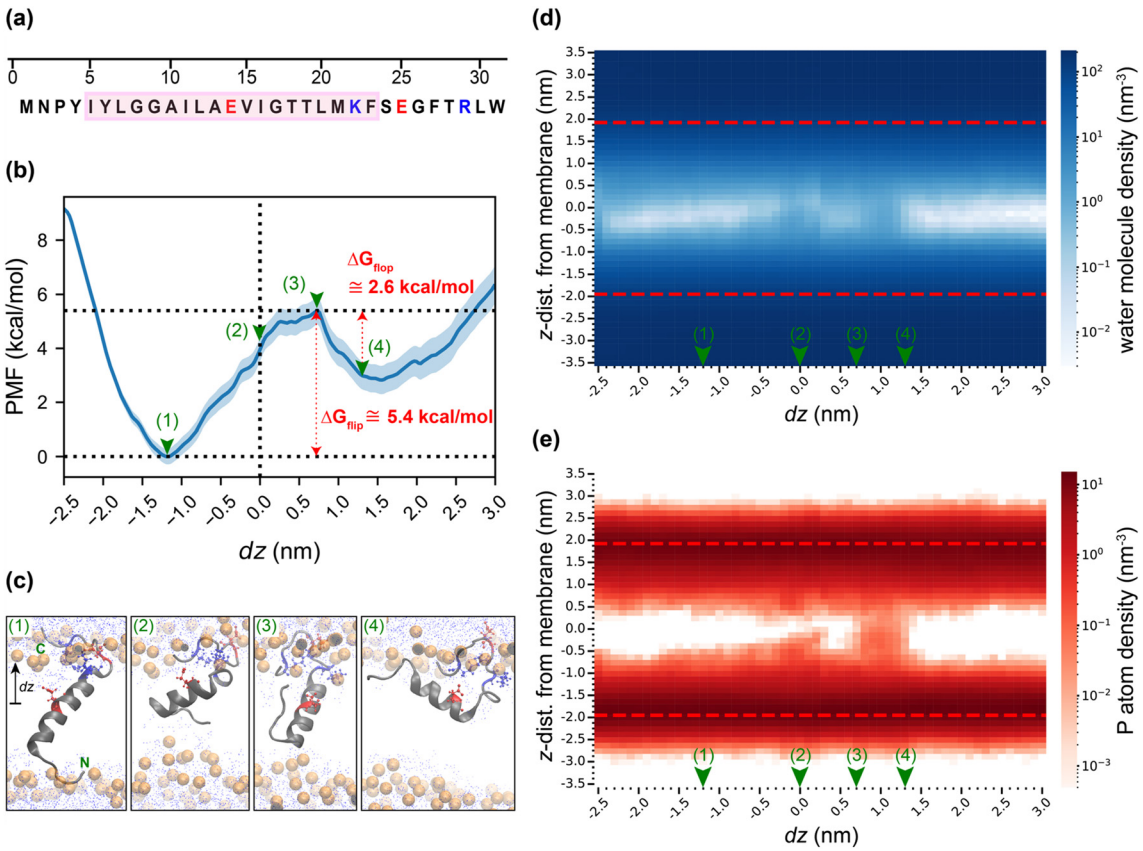

Fig. 3 Analysis of flipping for the truncated N-peptide-E14-charged (N-pep-charge). (a) Amino-acid sequence of N-pep-charge. The index of each amino acid with respect to the whole EmrE monomer sequence is shown above the residue. The transmembrane helix (TMH) of the peptide is highlighted with the pink box. Residues colored in blue and red are positively and negatively charged, respectively. E14 is charged in this sequence. (b) Potential of mean force (PMF) as a function of the z-component of the distance between the COM of the N-terminal loop and the center of the membrane, dz. The midplane of the membrane is at dz = 0 nm. The blue shaded area indicates the standard deviation computed by bootstrapping. (c) Simulation snapshots of N-pep-charge flipping. Each numbered snapshot corresponds to a representative configuration for the value of dz marked by a green arrowhead and corresponding number on the PMF curve in (b). The N-pep-charge is gray, positively charged amino acids are blue, negatively charged amino acids are red, phosphorus atoms of lipid head groups are orange, water molecules are blue dots, and lipid tails are not shown to aid visualization. The termini of the truncated peptide are labeled with green "N" and "C". (d) Heatmap of water molecule number densities and (e) heatmap of phosphorus atom number densities as a function of dz, following the same definition as Fig. 2.

in Fig. S15†). Partial unfolding at G17 continued until the PMF local minimum at $dz \approx 1.3$ nm which corresponds to a state in which the helical segment was embedded in only the upper bilayer leaflet (Fig. 3c and S15†). The energy barrier for the N-terminal loop to flip back, or "flop," to its initial structure with a global PMF minimum at $dz \approx -1.2$ nm was $\Delta G_{\text{flop}} \cong 2.6$ kcal mol^{-1}, which is even smaller than ΔG_{flip} and substantially smaller than ΔG_{flip} of the N-loop. These substantially reduced free energy barriers for flipping and flopping indicate the impact of the helical segment on the local chemical environment.

Distinct differences in water content and membrane structure (Fig. 3d and e) were observed during the flipping of the N-pep-charge peptide compared to the N-loop. Examination of the water densities and phosphorus atom densities for $dz < -1.2$ nm (*i.e.*, prior to flipping) shows that both water and phosphorus densities have increased values closer to the bilayer midplane than for the N-loop system, indicating that the average thickness of the DMPC bilayer was smaller in the N-pep-charge system than in the N-loop system. This difference can be attributed to electrostatic interactions between the charged E14 of the helical segment and water molecules and phosphorus head groups, leading to local membrane disruptions even at the global PMF minimum as shown in Fig. 3c. As a result, although the water density near the bilayer midplane increases with dz during flipping because some water molecules are dragged into the membrane, there is no large and sudden increase in the amount of water in the membrane as observed for the N-loop. Consequently, the value of ΔG_{flip} is smaller for N-pep-charge than N-loop since the deformation of the bilayer during flipping is reduced because of the pre-existing water defect and deformation promoted by the embedded helical segment. The snapshots in Fig. 3c similarly illustrate the N-loop accessing the pre-existing water defect near E14 during flipping. These observations are similar to deformations in membrane structure and water content that were previously observed for a simple TMH with a charged residue at its center,[77] which exhibited a sizable decrease in the free energy barrier for translocation depending upon the protonation state of a central aspartate residue due to stabilization of water defects.[38,39] Such deformations, along with the partial unfolding of the TMH1, may effectively stabilize water defects during the flipping process so that ΔG_{flip} of the N-pep-charge with 31 residues can be smaller than ΔG_{flip} of the N-loop with only 4 residues. These results suggest that it is the relative hydrophilicity of TMH1 that promotes its flipping in the EmrE monomer.

3.3. Flipping of the hydrophobic C-terminal helical domain of EmrE

Since the prior analysis suggests that N-terminal TMH1 flipping is promoted by the marginal hydrophobicity of its helix, we next characterized the flipping of a truncated segment mimicking the C-terminal TMH4 of EmrE, which is more hydrophobic (and thus typical of TMHs) and was not experimentally observed to flip.[32] Fig. 4a shows the sequence of TMH4 and its two flanking loops that comprise the truncated C-terminal segment (C-pep). Fig. 4b shows that the PMF for the flipping of C-pep is a monotonically increasing function of dz with only small, comparable local minima at $dz \approx 1.0$ nm and $dz \approx 2.2$ nm. The global minimum corresponds to the transmembrane state as expected given the hydrophobicity of TMH4; we attribute the lack of a deep minimum for positive values of dz to the strong preference for transmembrane embedding for the hydrophobic helix (Fig. S1†). ΔG_{flip} was ~12.1 kcal mol^{-1}, which is significantly larger than ΔG_{flip} for either the N-loop or N-pep-charge. The segment remained helical and continuously tilted during the flipping process (Fig. 4c and S15†).

The simulation snapshots in Fig. 4c reveal that flipping leads to the formation of a large bilayer defect at the PMF maximum. Fig. 4d and e indicate that the average thickness of the membrane of C-pep system remained larger than the case of N-pep-charge prior to flipping, likely because the bilayer structure was not affected by the hydrophobic TMH4. Therefore, flipping of the TMH requires the sudden permeation of a large number of water molecules into the center of the bilayer as the hydrophilic charged C-terminal loop drags solvent molecules along its pulled trajectory (Fig. 4c and d). Consequently, compared to the previous cases of N-loop and N-pep-charge systems, a more sizable membrane perturbation that resembles transient pore formation was observed during the flipping of C-pep (Fig. 4c and e). Both the intrusion of a large amount of water and the associated disruption of the membrane would account for the higher free energy barrier for flipping for C-pep. Therefore, multiple mechanistic changes that were energetically unfavorable occurred during the flipping of the truncated C-pep across the bilayer which is consistent with the stable topology of the C-terminal TMH4 domain of the EmrE monomer.

Based on the high flipping free energy barrier for the hydrophobic C-pep, we hypothesized that protonating the E14 residue in the N-terminal TMH1 (to increase its effective hydrophobicity) might similarly increase its flipping free energy barrier. Fig. S13† shows the resulting PMF, simulation snapshots, and water/phosphorus atom number densities for the flipping of a segment of the N-terminal TMH1 with a neutral E14 residue (N-pep-neut). These results are similar to those of C-pep; as TMH1 loses its charged residue at the center of the helix, the free energy barrier for flipping is more comparable to the barrier for flipping of the C-pep, no local minimum is observed for positive values of dz indicating a strong preference for the transmembrane state, and the mechanistic features captured during the flipping resemble those of C-pep, including the formation of a transient pore in the membrane to allow a substantial influx of water molecules and lipid phosphate groups into the hydrophobic core of the bilayer. Such a dramatic change due to only the protonation of E14 corroborates the hypothesis that, rather

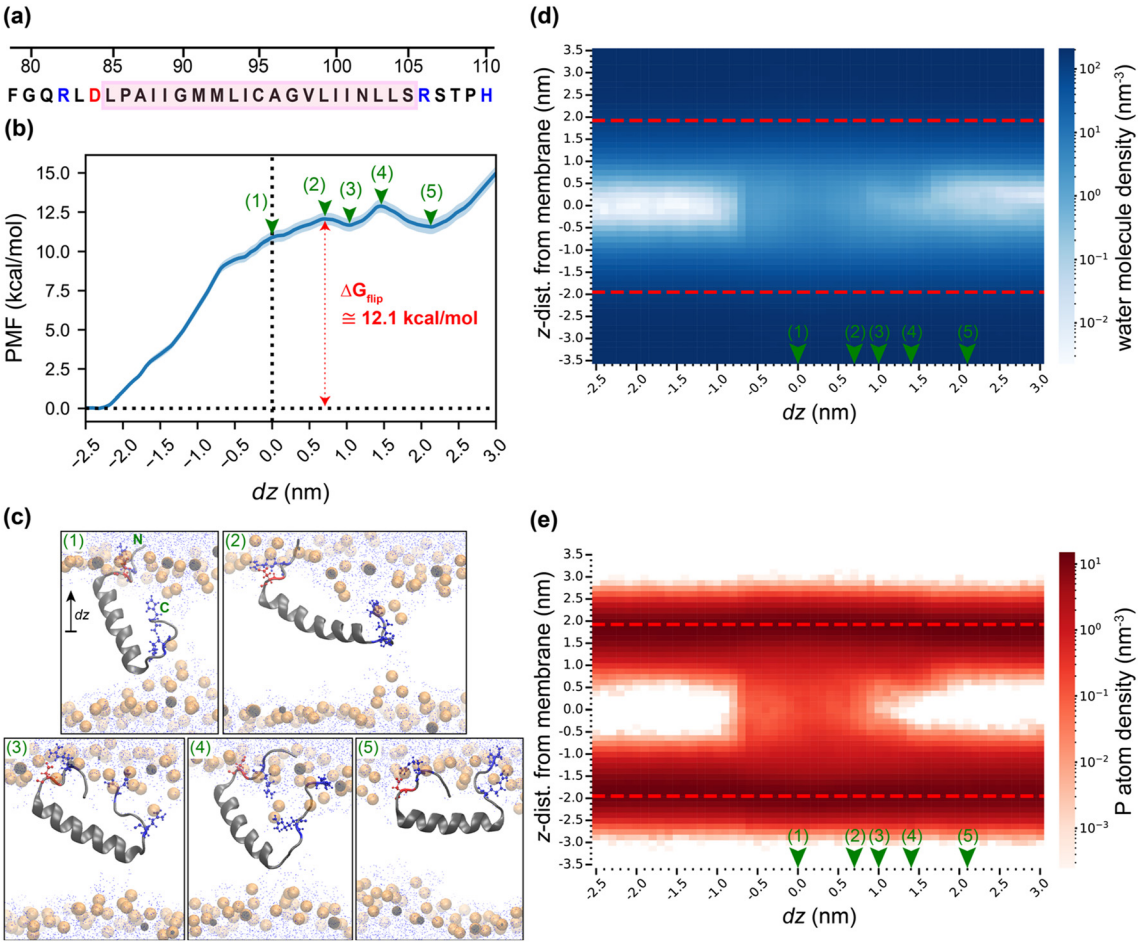

Fig. 4 Analysis of flipping for the truncated C-terminal peptide (C-pep). (a) Amino-acid sequence of C-pep. The index of each amino acid with respect to the whole EmrE monomer sequence is shown above the residue. The transmembrane helical (TMH) domain is highlighted with the pink box. Residues colored in blue and red are positively and negatively charged, respectively. (b) Potential of mean force (PMF) as a function of the *z*-component of the distance between the COM of the C-terminal loop and the center of the membrane, *dz*. The midplane of the membrane is at *dz* = 0 nm. The blue shaded area indicates the standard deviation computed by bootstrapping. (c) Simulation snapshots of C-pep flipping. Each numbered snapshot corresponds to a representative configuration for the value of *dz* marked by a green arrowhead and corresponding number on the PMF curve in (b). The C-pep is gray, positively charged amino acids are blue, negatively charged amino acid is red, phosphorus atoms of lipid head groups are orange, water molecules are blue dots, and lipid tails are not shown to aid visualization. The termini of the truncated peptide are labeled with green "N" and "C". (d) Heatmap of water molecule number densities and (e) heatmap of phosphorus atom number densities as a function of *dz*, following the same definition as Fig. 2.

than the marginally hydrophilic N-loop, it is the marginally hydrophobic TMH1 of EmrE that primarily accounts for the observed flipping of the N-terminal of the monomer, with E14 playing the critical role in determining the hydrophobicity of TMH1 *via* its protonation state. Specifically, the charged E14 residue promotes the deformation of the local membrane thickness and promotes the permeation of water molecules into the membrane prior to flipping, thereby decreasing the free energy cost associated with creating a water defect.[38,39,44,47,48,81,82]

3.4. Flipping of N- and C-terminal loops of the complete EmrE monomer.

The results of sections 3.1–3.3 indicate that the truncated N-terminal peptide with a deprotonated E14 residue has a smaller flipping free energy barrier than either its isolated N-terminal loop or a more hydrophobic C-terminal peptide (with charged flanking loops). Analysis of water content and bilayer deformation suggests that this lower barrier could be attributed to the E14 residue, which confers some hydrophilicity to the TMH and promotes higher membrane water content and pre-existing membrane deformation when the TMH is in its initial transmembrane state prior to flipping. We next sought to understand what sequence features affect flipping in the more complex chemical environment near the complete EmrE monomer to see to what extent the presence of other TMHs influences flipping. We thus performed the same enhanced sampling simulations and analysis for the flipping of both the N- and C-terminal TMHs of the complete EmrE monomer system to compare against the truncated segments.

Fig. 5 shows that analysis and observations for the EmrE monomer are largely consistent with the thermodynamic and mechanistic patterns observed for the truncated segments. The free energy barrier for flipping (Fig. 5a and c) is much larger for the C-terminal (≅18.8 kcal mol^{-1}) than for the N-terminal (≅9.2 kcal mol^{-1}) TMH, noting that E14 was treated as deprotonated and thus charged. The overall shapes of the PMF plots for the flipping of each terminal resemble those from the truncated systems (Fig. 3b and 4b). Pre-existing deformations in water and membrane structures are observed in both cases (Fig. 5b and d and S14†) due to the charged E14 residues, with greater deformation at the upper leaflet. We attribute this asymmetry in deformations to a pre-existing pore-like local environment at the upper leaflet formed by TMH1, TMH2, and TMH3 in their initial transmembrane topology. The magnitude of this deformation, in terms of the average membrane thickness, is larger in the EmrE monomer than in the truncated peptide systems, presumably due to the asymmetry in the transmembrane topology of EmrE compared to the truncated single helices. Only the N-terminal TMH crosses through this pre-existing water defect during flipping, however; this difference in local chemical environment leads to the significant difference in the energetic profiles for N- and C-terminal loop flipping.

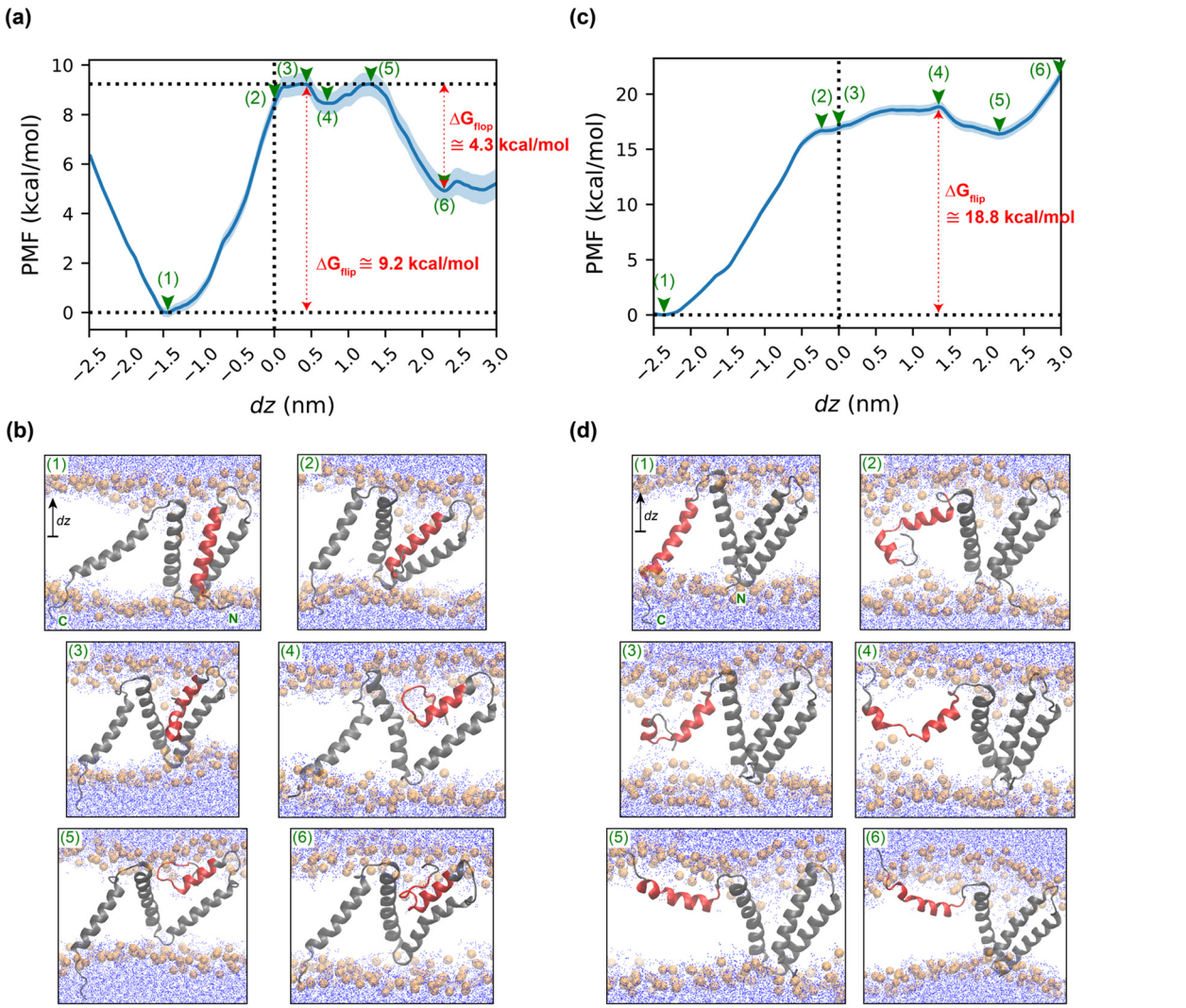

Fig. 5 Analysis of flipping for the N- and C-terminal loops of EmrE monomer. (a) Potential of mean force (PMF) as a function of the *z*-component of the distance between the COM of the N-terminal loop and the center of the membrane, *dz*. The midplane of the membrane is at *dz* = 0 nm. The blue shaded area indicates the standard deviation computed by bootstrapping. (b) Simulation snapshots of EmrE N-terminal TMH1 flipping. Each snapshot corresponds to a representative configuration for the value of *dz* marked by a green arrowhead on the PMF curve in (a). The EmrE monomer is gray, TMH1 is red, phosphorus atoms of lipid head groups are orange, water molecules are blue dots, and lipid tails are not shown to aid visualization. The termini of the protein are labeled with green "N" and "C". (c) PMF as a function of the *dz* of the distance between the COM of the C-terminal loop and the center of the membrane. The midplane of the membrane is at *dz* = 0 nm. The blue shaded area indicates the standard deviation computed by bootstrapping. (d) Simulation snapshots of EmrE C-terminal TMH4 flipping. Each numbered snapshot corresponds to a representative configuration for the value of *dz* marked by a green arrowhead and corresponding number on the PMF curve in (c). The EmrE monomer is gray, TMH4 is red, and other visualizations follow same as (b).

Similar to the truncated peptide systems, these results indicate that the charged E14 residue minimizes further deformation in water and membrane structures during the flipping of the N-terminal loop due to the pre-existing water deformation around TMH1, while no such local environment is provided for C-terminal flipping.

While the shape and trends in the PMFs for the EmrE monomer are the same as truncated segments, the barriers to flipping and flopping are larger for the N- and C-terminal TMHs compared to the equivalent truncated segments, which we attribute in part to variations in the local membrane environment due to the larger monomer. We also investigated another feature of the local chemical environment that is unique to the EmrE monomer: interhelical H-bond networks. Unlike in the truncated segment, N-terminal loop flipping for the monomer requires TMH1 to break stable H-bonds that are formed with other helices when in the transmembrane state (Fig. 6a, with simulation snapshots shown in Fig. 5b). Notably, among interhelical H-bonds with TMH1, the H-bond between TMH1 and TMH2 (Fig. 6a) is the most stable interaction when EmrE is embedded inside the membrane. Since interhelical H-bonds are known to stabilize the transmembrane topology of IMPs,[83–88] it is somewhat surprising that the flipping of the N-terminal helix, which forms a stable H-bond with an adjacent TMH, requires a much smaller free energy change than the flipping of the C-terminal helix, which shows almost no H-bonds with other helices (Fig. 6b, with simulation snapshots shown in Fig. 5d). Changes in the monomer's conformations and local chemical environments observed during each flipping process can explain this unexpected pattern in flipping barrier. Specifically, the simulation snapshots show that the stable H-bond between TMH1 and TMH2 does not significantly hinder the flipping of the EmrE N-terminal loop because TMH2 tilts with TMH1 while TMH1 partially unfolds into the loop during the flipping (Fig. 5b). This relaxation of the whole monomer helps lower the energetic barrier for the process. The decrease in H-bonding between TMH1 and TMH2 is partially compensated by the formation of an H-bond between TMH1 and TMH3 after flipping occurs, leading to only a small decrease in overall H-bonding. However, this change in interhelical H-bonding likely still contributes to the greater energetic barrier for flipping of the N-terminal loop of the EmrE monomer than the truncated loop (Fig. 2a) or the peptide with TMH1 (Fig. 3b). These results point to potential design rules for influencing flipping processes by introducing functional groups capable of forming intramembrane H-bonds, particularly for larger synthetic materials like nanoparticles or polymers.

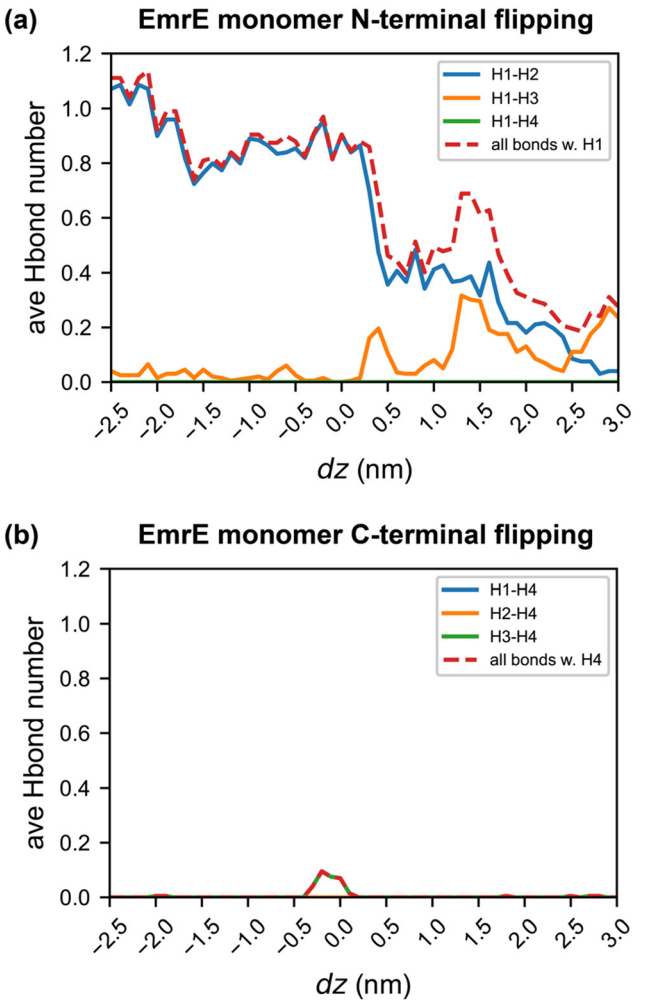

Fig. 6 Interhelical hydrogen bonding patterns of flipping for the N- and C-terminal loops of EmrE monomer. (a) Time-averaged number of hydrogen bonds between TMH1 and other helices for the N-terminal loop flipping as a function of *dz*. The legend "H1–H2" indicates H-bonds between TMH1 and TMH2 and other legends follow the same definition. The red dashed line indicates all interhelical H-bonds of TMH1. (b) Time-averaged number of hydrogen bonds between TMH4 and other helices for the C-terminal loop flipping as a function of *dz*. The legend "H1–H4" indicates H-bonds between TMH1 and TMH4 and other legends follow the same definition. The red dashed line indicates all interhelical H-bonds of TMH4.

3.5. Quantitative analysis of hydrogen bonds between transmembrane helices of EmrE

The analysis in the preceding section indicates that interhelical H-bonds can affect flipping in the EmrE monomer. Since interhelical H-bonding has been demonstrated both experimentally and computationally to be one of the essential driving forces that facilitates the association of hydrophobic TMHs in lipid bilayers,[83–88] we hypothesized that H-bonding between TMHs could be particularly relevant to stabilizing the EmrE dimer to inhibit the ability of the N-terminal helix to flip, as observed experimentally, due to its association with other helices. We further hypothesized that the protonation state of the membrane-exposed E14 residue, previously shown to promote flipping, could also affect interhelical H-bonding, thereby providing new insight into potential design rules for tuning the stability of transmembrane segments. To

investigate these hypotheses, we compared the time-averaged number of H-bonds between the TMHs of EmrE for the membrane-embedded monomer and dimer states (Fig. 7a). The protonation states of the E14 residues in the EmrE dimer were considered to change as a pair since the functional dimer is known to simultaneously alternate the protonation state of E14 of each monomer, whether both protonated or deprotonated, to perform the efflux of drug-like molecules coupled with proton import.[52,78,89]

For the EmrE monomer in its equilibrated state (Fig. 7b, Table S2†), multiple but transient interhelical H-bonds between TMHs were observed (thin green lines in Fig. 7b) when E14 was deprotonated (*i.e.*, charged), while a relatively persistent H-bond between TMHs, particularly between the side chain of TMH1 E14 and the carbonyl oxygen of TMH3 W63 (Table S3†), was observed when E14 was protonated (thicker green lines in Fig. 7b). For the E14-deprotonated monomer, although the time-averaged number of H-bonds between TMH1 and TMH2 is relatively high (~0.971; see Table S2†) compared to other interhelical H-bonds, this number consists of numerous transient H-bonds compared to the case when E14 is protonated with a persistent H-bond between TMH1 E14 and TMH3 W63 (Table S3†). These multiple but transient H-bonds may not significantly stabilize the transmembrane topology of the EmrE monomer (Fig. 6a), thereby allowing the flipping of the N-terminal loop. We expect that this difference in interhelical H-bonding depending on the protonation state of E14 would further exacerbate the energetic difference in flipping of the EmrE monomer when E14 is deprotonated *vs.* protonated (Fig. 3b and S13b†) since both the higher flipping barrier and persistent interhelical H-bonds would inhibit the flipping of TMH1 if E14 is protonated. This analysis again points to the charge of E14 of EmrE as critical to promoting flipping.

For the EmrE dimer in its equilibrated membrane-embedded state (Fig. 7c, Tables S4 and S5†), persistent H-bonds between TMH1 of chain A and TMH3 of chain B, predominantly residues E14 and Y60 (Table S6†), were observed for the dimer with deprotonated E14 residues (thick green lines in Fig. 7c). These interactions weakened significantly when E14 residues were protonated (Table S7†). Notably, a persistent H-bond between TMH3 of chain A and TMH1 of chain B, with the same residue pair Y60 and E14, was observed for the dimer with protonated E14 residues (Fig. 7c, Tables S5 and S7†). Similar to the EmrE monomer, persistent interhelical H-bonds within each monomer, with the same residue pair E14 and W63, were observed when E14 residues of the dimer were protonated (Fig. 7c, Tables S4 and S7†). These patterns in interhelical hydrogen bonding were also found to persist when using steered MD simulations to force the flipping of the N-terminal helix of either the EmrE monomer or dimer (Fig. 6a and S16, Tables S8 and S9†). The observation that E14 plays the critical role in interhelical H-bonding for EmrE in its monomer and dimer state agrees with previous findings that polar residues at the center of transmembrane helices have the most significant per-residue

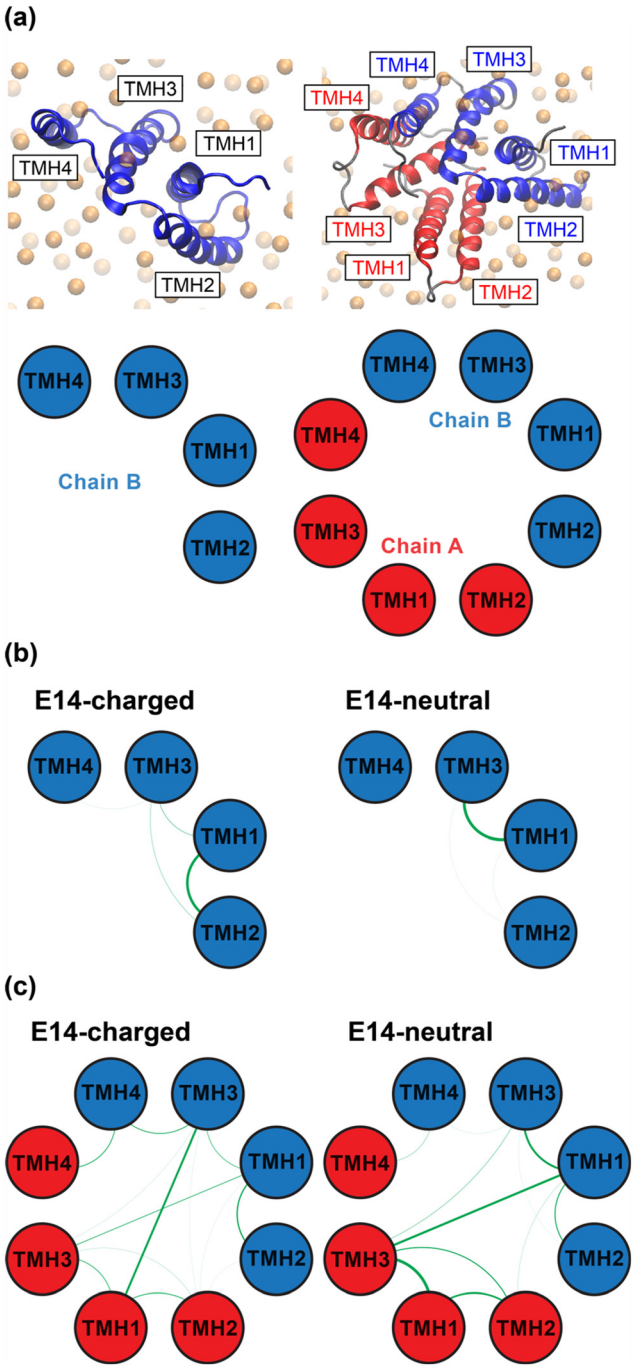

Fig. 7 Interhelical hydrogen bonding patterns in EmrE. (a) Structures of the EmrE monomer (left) and dimer (right) viewed from above the membrane. Chain A is in red, chain B is in blue, and phosphorus atoms are in orange. Topological maps of TMHs corresponding to each structure are shown below with helices numbered by the order in which they appear in the primary sequence. (b) Topological maps of interhelical hydrogen bonds for the EmrE monomer with E14 deprotonated (E14-charged, at left) or protonated (E14-neutral, at right). Green lines connecting the TMHs represent hydrogen bonds and the line thickness quantifies their persistence based on the time-averaged number of the bonds during a 500 ns simulation (values in Table S2†). (c) Topological maps of interhelical hydrogen bonds for the EmrE dimer with E14 deprotonated (E14-charged, at left) or protonated (E14-neutral, at right). Green lines connecting the TMHs represent hydrogen bonds as in (b). Both intra- and intermonomer hydrogen bonds are marked (numerical values in Tables S4 and S5†).

contribution to the free energy of helix association as a function of helix–helix distance due to strong interhelical interactions.[84,86,88] Based on the strength of these interhelical H-bonds, and the prior analysis of the effect of H-bonding on flipping in the EmrE monomer, we conclude that dimerization likely arrests flipping by promoting the formation of persistent H-bonds between TMHs.

4. Conclusions

In this work, we use molecular simulations to investigate what sequence features affect the flipping of the N-terminal helix (TMH1) of EmrE across a single-component lipid membrane, and why flipping is inhibited upon dimerization, in order to suggest bioinspired design rules for enhancing membrane translocation. Comparing free energy barriers for flipping systematically truncated EmrE peptides indicates that the lowest free energy barrier for flipping is observed for the marginally hydrophobic TMH1 with a deprotonated (charged) E14 residue. Conversely, protonating E14 to increase TMH1 hydrophobicity leads to a free energy barrier similar to that of the more hydrophobic C-terminal helix, which is experimentally not observed to flip. Charged E14 stabilizes the water defect caused by the flipping of TMH1 to minimize the deformation to the membrane and avoid transient pore formation, as is observed for the other truncated segments. Additionally, quantitative analysis of interhelical H-bonding for the EmrE monomer and dimer indicates that increased hydrogen bonding upon dimerization would inhibit flipping. These results suggest multiple bioinspired design rules for synthetic materials capable of flipping hydrophilic or charged groups across the bilayer: (1) introducing hydrophilic, and particularly charged, membrane-exposed functional groups can promote flipping by stabilizing water defects, (2) tuning the hydrophobicity of a transmembrane domain (*e.g.*, modulating the protonation state of membrane-exposed functional groups) can impact flipping thermodynamics more substantially than tuning the hydrophilicity of the group that is flipping, and (3) adding functional groups capable of intra-membrane H-bonding can inhibit flipping, or alternatively stabilize membrane-embedded states. We expect that these design rules will be valuable for engineering the properties of synthetic peptides,[16–18] nanomaterials,[19] or polymers[20] with multiple functional groups, particularly for applications in intracellular delivery.

Beyond these design rules, these findings also provide biophysical insight into factors affecting topological changes in naturally occurring IMPs. While folding in true biological membranes likely involves factors including membrane asymmetry, protein chaperones, or other membrane components such as lipopolysaccharides,[90,91] our findings highlight the importance of the marginal hydrophobicity of the N-terminal TMH1 as an intrinsic factor that facilitates the flipping of the EmrE monomer. Considering the paucity of glutamate residsues observed in transmembrane α-helices,[79,80] both the presence of E14 itself and its location at the center of TMH1 may create a synergy that confers the unusual dynamic membrane topology to EmrE monomers. Our results further indicate that the protonation state of E14 shifts the H-bonding patterns between TMHs in EmrE; similar shifts have been shown experimentally to introduce a kink or conformation change to helices.[92] Therefore, the H-bonding pattern of the EmrE monomer with the deprotonated E14 may confer considerable flexibility into TMH1 that permits the transient kink at G17 (Fig. 3c) and lowers the energetic barrier for the dynamic flip-flop of the N-terminal helix. After dimerization, however, the shifted hydrogen bonding pattern of EmrE significantly stabilizes its whole structure regardless of the protonation state of E14 so that the dimer losses its dynamic membrane topology. The identification of these behaviors for a naturally occurring transmembrane protein suggests that flipping may also be important to the folding and topogenesis of other naturally occurring proteins. For example, the folding and unfolding of various bacterial outer membrane proteins in synthetic, neutral, single-component lipid vesicles is kinetically controlled by factors similar to the ones that affect charge translocation, including membrane thickness[93] and the presence of membrane defects,[94] indicating that folding may require charged or hydrophilic groups to cross the membrane.[95] These results may thus inspire future investigation of the extent to which marginally hydrophobic domains are associated with topology changes in diverse proteins as part of protein folding pathways. Future work will also build upon this study's investigation of flipping in a single-component DMPC lipid membrane to consider the impact of membrane composition on flipping behavior, recognizing that biological membranes include a large number of components and can be asymmetric in composition.[96]

Data availability

The molecular dynamics simulation data, including starting configurations, trajectories, and analyzed output, are available at the following Dryad repository: **https://doi.org/10.5061/dryad.f1vhhmh7d**.

Conflicts of interest

There are no conflicts to declare.

Acknowledgements

This material is based upon work supported by the National Science Foundation under Grant No. MCB-1817292. This work used the Advanced Cyberinfrastructure Coordination Ecosystem: Services & Support (ACCESS), which is supported by the National Science Foundation under Grant No. 2138307.

References

1 S. H. White and W. C. Wimley, Membrane protein folding and stability: physical principles, *Annu. Rev. Biophys. Biomol. Struct.*, 1999, **28**(1), 319–365.

2 G. von Heijne, Membrane-protein topology, *Nat. Rev. Mol. Cell Biol.*, 2006, **7**(12), 909–918.

3 F. Cymer, G. von Heijne and S. H. White, Mechanisms of Integral Membrane Protein Insertion and Folding, *J. Mol. Biol.*, 2015, **427**(5), 999–1022, DOI: **10.1016/j.jmb.2014.09.014**.

4 J. L. Popot and D. M. Engelman, Membrane protein folding and oligomerization: the two-stage model, *Biochemistry*, 1990, **29**(17), 4031–4037, DOI: **10.1021/bi00469a001**.

5 J. LeBarron and E. London, Highly Hydrophilic Segments Attached to Hydrophobic Peptides Translocate Rapidly across Membranes, *Langmuir*, 2016, **32**(41), 10752–10760, DOI: **10.1021/acs.langmuir.6b02597**.

6 M. Bogdanov, J. Xie, P. Heacock and W. Dowhan, To flip or not to flip: lipid–protein charge interactions are a determinant of final membrane protein topology, *J. Cell Biol.*, 2008, **182**(5), 925–935.

7 K. Öjemalm, K. K. Halling, I. Nilsson and G. von Heijne, Orientational preferences of neighboring helices can drive ER insertion of a marginally hydrophobic transmembrane helix, *Mol. Cell*, 2012, **45**(4), 529–540.

8 S. Seppälä, J. S. Slusky, P. Lloris-Garcerá, M. Rapp and G. von Heijne, Control of Membrane Protein Topology by a Single C-Terminal Residue, *Science*, 2010, **328**(5986), 1698–1700, DOI: **10.1126/science.1188950**, (accessed 2024/01/24).

9 R. C. Van Lehn, B. Zhang and T. F. Miller III, Regulation of multispanning membrane protein topology via post-translational annealing, *eLife*, 2015, **4**, e08697, DOI: **10.7554/eLife.08697**.

10 N. B. Woodall, Y. Yin and J. U. Bowie, Dual-topology insertion of a dual-topology membrane protein, *Nat. Commun.*, 2015, **6**(1), 8099, DOI: **10.1038/ncomms9099**.

11 Y. Lu, I. R. Turnbull, A. Bragin, K. Carveth, A. S. Verkman and W. R. Skach, Reorientation of aquaporin-1 topology during maturation in the endoplasmic reticulum, *Mol. Biol. Cell*, 2000, **11**(9), 2973–2985.

12 F. X. Contreras, L. Sánchez-Magraner, A. Alonso and F. M. Goñi, Transbilayer (flip-flop) lipid motion and lipid scrambling in membranes, *FEBS Lett.*, 2010, **584**(9), 1779–1786.

13 O. A. Andreev, D. M. Engelman and Y. K. Reshetnyak, Targeting diseased tissues by pHLIP insertion at low cell surface pH, *Front. Physiol.*, 2014, **5**, 73407.

14 O. A. Andreev, A. G. Karabadzhak, D. Weerakkody, G. O. Andreev, D. M. Engelman and Y. K. Reshetnyak, pH (low) insertion peptide (pHLIP) inserts across a lipid bilayer as a helix and exits by a different path, *Proceedings of the National Academy of Sciences*, 2010, **107**(9), 4081–4086.

15 I. Vorobyov, Timothy E. Olson, Jung H. Kim, Roger E. Koeppe, Olaf S. Andersen and Toby W. Allen, Ion-Induced Defect Permeation of Lipid Membranes, *Biophys. J.*, 2014, **106**(3), 586–597, DOI: **10.1016/j.bpj.2013.12.027**.

16 S. C. Povilaitis, A. Fathizadeh, M. Kogan, R. Elber and L. J. Webb, Design of peptides for membrane insertion: The critical role of charge separation, *J. Phys. Chem. B*, 2022, **126**(34), 6454–6463.

17 R. Elber, Defect formation and peptide permeation across phospholipid membranes, *J. Phys. Chem. B*, 2023, **127**(37), 7810–7818.

18 Z. Kang, Q. Liu, Z. Zhang, Y. Zheng, C. Wang, Z. Pan, Q. Li, Y. Liu and L. Shi, Arginine-Rich Polymers with Pore-Forming Capability Enable Efficient Intracellular Delivery via Direct Translocation Across Cell Membrane, *Adv. Healthcare Mater.*, 2022, **11**(14), 2200371.

19 R. C. Van Lehn, P. U. Atukorale, R. P. Carney, Y.-S. Yang, F. Stellacci, D. J. Irvine and A. Alexander-Katz, Effect of particle diameter and surface composition on the spontaneous fusion of monolayer-protected gold nanoparticles with lipid bilayers, *Nano Lett.*, 2013, **13**(9), 4060–4067.

20 Y.-W. Lee, D. C. Luther, R. Goswami, T. Jeon, V. Clark, J. Elia, S. Gopalakrishnan and V. M. Rotello, Direct cytosolic delivery of proteins through coengineering of proteins and polymeric delivery vehicles, *J. Am. Chem. Soc.*, 2020, **142**(9), 4349–4355.

21 S. Schuldiner, EmrE, a model for studying evolution and mechanism of ion-coupled transporters, *Biochim. Biophys. Acta, Proteins Proteomics*, 2009, **1794**(5), 748–762, DOI: **10.1016/j.bbapap.2008.12.018**.

22 I. Nasie, S. Steiner-Mordoch, A. Gold and S. Schuldiner, Topologically Random Insertion of EmrE Supports a Pathway for Evolution of Inverted Repeats in Ion-coupled Transporters*, *J. Biol. Chem.*, 2010, **285**(20), 15234–15244, DOI: **10.1074/jbc.M110.108746**.

23 Y.-J. Chen, O. Pornillos, S. Lieu, C. Ma, A. P. Chen and G. Chang, X-ray structure of EmrE supports dual topology model, *Proc. Natl. Acad. Sci. U. S. A.*, 2007, **104**(48), 18999–19004, DOI: **10.1073/pnas.0709387104**, (accessed 2024/01/25).

24 M. Rapp, S. Seppälä, E. Granseth and G. von Heijne, Emulating Membrane Protein Evolution by Rational Design, *Science*, 2007, **315**(5816), 1282–1284, DOI: **10.1126/science.1135406**, (accessed 2024/01/25).

25 M. H. Saier Jr and I. T. Paulsen, Phylogeny of multidrug transporters, *Semin. Cell Dev. Biol.*, 2001, **12**(3), 205–213, DOI: **10.1006/scdb.2000.0246**.

26 I. T. Paulsen, R. A. Skurray, R. Tam, M. H. Saier Jr, R. J. Turner, J. H. Weiner, E. B. Goldberg and L. L. Grinius, The SMR family: a novel family of multidrug efflux proteins involved with the efflux of lipophilic drugs, *Mol. Microbiol.*, 1996, **19**(6), 1167–1175.

27 M. Rapp, E. Granseth, S. Seppälä and G. Von Heijne, Identification and evolution of dual-topology membrane proteins, *Nat. Struct. Mol. Biol.*, 2006, **13**(2), 112–116.

28 D. C. Bay, K. L. Rommens and R. J. Turner, Small multidrug resistance proteins: A multidrug transporter family that continues to grow, *Biochim. Biophys. Acta, Biomembr.*, 2008, **1778**(9), 1814–1838, DOI: **10.1016/j.bbamem.2007.08.015**.

29 A. A. Kermani, C. B. Macdonald, R. Gundepudi and R. B. Stockbridge, Guanidinium export is the primal function of SMR family transporters, *Proc. Natl. Acad. Sci. U. S. A.*, 2018, **115**(12), 3060–3065.
30 N. B. Woodall, S. Hadley, Y. Yin and J. U. Bowie, Complete topology inversion can be part of normal membrane protein biogenesis, *Protein Sci.*, 2017, **26**(4), 824–833, DOI: **10.1002/pro.3131**, (accessed 2024-01-25T06:27:20).
31 N. Fluman, V. Tobiasson and G. von Heijne, Stable membrane orientations of small dual-topology membrane proteins, *Proc. Natl. Acad. Sci. U. S. A.*, 2017, **114**(30), 7987–7992, DOI: **10.1073/pnas.1706905114**, (accessed 2024/01/25).
32 M. Seurig, M. Ek, G. von Heijne and N. Fluman, Dynamic membrane topology in an unassembled membrane protein, *Nat. Chem. Biol.*, 2019, **15**(10), 945–948.
33 M. Bogdanov, W. Dowhan and H. Vitrac, Lipids and topological rules governing membrane protein assembly, *Biochim. Biophys. Acta, Mol. Cell Res.*, 2014, **1843**(8), 1475–1488.
34 H. Vitrac, D. M. MacLean, V. Jayaraman, M. Bogdanov and W. Dowhan, Dynamic membrane protein topological switching upon changes in phospholipid environment, *Proc. Natl. Acad. Sci. U. S. A.*, 2015, **112**(45), 13874–13879.
35 J. Morstein, A. Capecchi, K. Hinnah, B. Park, J. Petit-Jacques, R. C. Van Lehn, J.-L. Reymond and D. Trauner, Medium-Chain Lipid Conjugation Facilitates Cell-Permeability and Bioactivity, *J. Am. Chem. Soc.*, 2022, **144**(40), 18532–18544, DOI: **10.1021/jacs.2c07833**.
36 C. A. Huang-Zhu, J. K. Sheavly, A. K. Chew, S. J. Patel and R. C. Van Lehn, Ligand Lipophilicity Determines Molecular Mechanisms of Nanoparticle Adsorption to Lipid Bilayers, *ACS Nano*, 2024, **18**(8), 6424–6437, DOI: **10.1021/acsnano.3c11854**.
37 C. G. Gahan, S. J. Patel, L. M. Chen, D. E. Manson, Z. J. Ehmer, H. E. Blackwell, R. C. Van Lehn and D. M. Lynn, Bacterial Quorum Sensing Signals Promote Large-Scale Remodeling of Lipid Membranes, *Langmuir*, 2021, **37**(30), 9120–9136, DOI: **10.1021/acs.langmuir.1c01204**.
38 S. J. Patel and R. C. Van Lehn, Analysis of Charged Peptide Loop-Flipping across a Lipid Bilayer Using the String Method with Swarms of Trajectories, *J. Phys. Chem. B*, 2021, **125**(22), 5862–5873, DOI: **10.1021/acs.jpcb.1c02810**.
39 S. J. Patel and R. C. Van Lehn, Characterizing the Molecular Mechanisms for Flipping Charged Peptide Flanking Loops across a Lipid Bilayer, *J. Phys. Chem. B*, 2018, **122**(45), 10337–10348, DOI: **10.1021/acs.jpcb.8b06613**.
40 H.-Y. Zhang, Q. Xu, Y.-K. Wang, T.-Z. Zhao, D. Hu and D.-Q. Wei, Passive Transmembrane Permeation Mechanisms of Monovalent Ions Explored by Molecular Dynamics Simulations, *J. Chem. Theory Comput.*, 2016, **12**(10), 4959–4969, DOI: **10.1021/acs.jctc.6b00695**.
41 C. Neale, C. Madill, S. Rauscher and R. Pomès, Accelerating Convergence in Molecular Dynamics Simulations of Solutes in Lipid Membranes by Conducting a Random Walk along the Bilayer Normal, *J. Chem. Theory Comput.*, 2013, **9**(8), 3686–3703, DOI: **10.1021/ct301005b**.
42 Y. Hu, S. Ou and S. Patel, Free Energetics of Arginine Permeation into Model DMPC Lipid Bilayers: Coupling of Effective Counterion Concentration and Lateral Bilayer Dimensions, *J. Phys. Chem. B*, 2013, **117**(39), 11641–11653, DOI: **10.1021/jp404829y**.
43 S. Dorairaj and T. W. Allen, On the thermodynamic stability of a charged arginine side chain in a transmembrane helix, *Proc. Natl. Acad. Sci. U. S. A.*, 2007, **104**(12), 4943–4948.
44 R. C. Van Lehn and A. Alexander-Katz, Grafting charged species to membrane-embedded scaffolds dramatically increases the rate of bilayer flipping, *ACS Cent. Sci.*, 2017, **3**(3), 186–195.
45 J. L. MacCallum, W. F. D. Bennett and D. P. Tieleman, Transfer of Arginine into Lipid Bilayers Is Nonadditive, *Biophys. J.*, 2011, **101**(1), 110–117, DOI: **10.1016/j.bpj.2011.05.038**.
46 C. Allolio, K. Baxova, M. Vazdar and P. Jungwirth, Guanidinium Pairing Facilitates Membrane Translocation, *J. Phys. Chem. B*, 2016, **120**(1), 143–153, DOI: **10.1021/acs.jpcb.5b10404**.
47 A. C. V. Johansson and E. Lindahl, Protein contents in biological membranes can explain abnormal solvation of charged and polar residues, *Proc. Natl. Acad. Sci. U. S. A.*, 2009, **106**(37), 15684–15689.
48 L. Bartoš, I. Kabelka and R. Vácha, Enhanced translocation of amphiphilic peptides across membranes by transmembrane proteins, *Biophys. J.*, 2021, **120**(11), 2296–2305.
49 T. Jin, S. J. Patel and R. C. Van Lehn, Molecular simulations of lipid membrane partitioning and translocation by bacterial quorum sensing modulators, *PLoS One*, 2021, **16**(2), e0246187.
50 M. B. Ulmschneider and M. S. P. Sansom, Amino acid distributions in integral membrane protein structures, *Biochim. Biophys. Acta, Biomembr.*, 2001, **1512**(1), 1–14, DOI: **10.1016/S0005-2736(01)00299-1**.
51 M. N. Mbaye, Q. Hou, S. Basu, F. Teheux, F. Pucci and M. Rooman, A comprehensive computational study of amino acid interactions in membrane proteins, *Sci. Rep.*, 2019, **9**(1), 12043, DOI: **10.1038/s41598-019-48541-2**.
52 A. A. Shcherbakov, G. Hisao, V. S. Mandala, N. E. Thomas, M. Soltani, E. A. Salter, J. H. Davis, K. A. Henzler-Wildman and M. Hong, Structure and dynamics of the drug-bound bacterial transporter EmrE in lipid bilayers, *Nat. Commun.*, 2021, **12**(1), 172, DOI: **10.1038/s41467-020-20468-7**.
53 J. V. Vermaas, S. B. Rempe and E. Tajkhorshid, Electrostatic lock in the transport cycle of the multidrug resistance transporter EmrE, *Proc. Natl. Acad. Sci. U. S. A.*, 2018, **115**(32), E7502–E7511.
54 R. B. Best, X. Zhu, J. Shim, P. E. M. Lopes, J. Mittal, M. Feig and A. D. MacKerell Jr, Optimization of the Additive CHARMM All-Atom Protein Force Field Targeting Improved Sampling of the Backbone ϕ, ψ and Side-Chain $\chi1$ and $\chi2$

Dihedral Angles, *J. Chem. Theory Comput.*, 2012, **8**(9), 3257–3273, DOI: **10.1021/ct300400x**.

55 J. B. Klauda, R. M. Venable, J. A. Freites, J. W. O'Connor, D. J. Tobias, C. Mondragon-Ramirez, I. Vorobyov, A. D. MacKerell Jr. and R. W. Pastor, Update of the CHARMM All-Atom Additive Force Field for Lipids: Validation on Six Lipid Types, *J. Phys. Chem. B*, 2010, **114**(23), 7830–7843, DOI: **10.1021/jp101759q**.

56 J. Huang, S. Rauscher, G. Nawrocki, T. Ran, M. Feig, B. L. De Groot, H. Grubmüller and A. D. MacKerell Jr, CHARMM36m: an improved force field for folded and intrinsically disordered proteins, *Nat. Methods*, 2017, **14**(1), 71–73.

57 S. Jo, T. Kim, V. G. Iyer and W. Im, CHARMM-GUI: A web-based graphical user interface for CHARMM, *J. Comput. Chem.*, 2008, **29**(11), 1859–1865, DOI: **10.1002/jcc.20945**.

58 S. Jo, T. Kim and W. Im, Automated Builder and Database of Protein/Membrane Complexes for Molecular Dynamics Simulations, *PLoS One*, 2007, **2**(9), e880, DOI: **10.1371/journal.pone.0000880**.

59 E. L. Wu, X. Cheng, S. Jo, H. Rui, K. C. Song, E. M. Dávila-Contreras, Y. Qi, J. Lee, V. Monje-Galvan and R. M. Venable, *et al.*, CHARMM-GUI Membrane Builder toward realistic biological membrane simulations, *J. Comput. Chem.*, 2014, **35**(27), 1997–2004, DOI: **10.1002/jcc.23702**, (accessed 2023/10/30).

60 J. Lee, X. Cheng, J. M. Swails, M. S. Yeom, P. K. Eastman, J. A. Lemkul, S. Wei, J. Buckner, J. C. Jeong and Y. Qi, *et al.*, CHARMM-GUI Input Generator for NAMD, GROMACS, AMBER, OpenMM, and CHARMM/OpenMM Simulations Using the CHARMM36 Additive Force Field, *J. Chem. Theory Comput.*, 2016, **12**(1), 405–413, DOI: **10.1021/acs.jctc.5b00935**.

61 M. A. Lomize, I. D. Pogozheva, H. Joo, H. I. Mosberg and A. L. Lomize, OPM database and PPM web server: resources for positioning of proteins in membranes, *Nucleic Acids Res.*, 2012, **40**(Database issue), D370–D376, DOI: **10.1093/nar/gkr703 From NLM**.

62 H. J. C. Berendsen, J. P. M. Postma, W. F. Van Gunsteren, A. Dinola and J. R. Haak, Molecular dynamics with coupling to an external bath, *J. Chem. Phys.*, 1984, **81**(8), 3684–3690, DOI: **10.1063/1.448118**, (accessed 2023-11-17T22:04:02).

63 M. J. Abraham, T. Murtola, R. Schulz, S. Páll, J. C. Smith, B. Hess and E. Lindahl, GROMACS: High performance molecular simulations through multi-level parallelism from laptops to supercomputers, *SoftwareX*, 2015, **1**, 19–25.

64 U. Essmann, L. Perera, M. L. Berkowitz, T. Darden, H. Lee and L. G. Pedersen, A smooth particle mesh Ewald method, *J. Chem. Phys.*, 1995, **103**(19), 8577–8593, DOI: **10.1063/1.470117**, (accessed 2023-11-17T23:28:50).

65 B. Hess, H. Bekker, H. J. C. Berendsen and J. G. E. M. Fraaije, LINCS: A linear constraint solver for molecular simulations, *J. Comput. Chem.*, 1997, **18**(12), 1463–1472, DOI: **10.1002/(sici)1096-987x(199709)18:12<1463::aid-jcc4>3.0.co;2-h**, (accessed 2023-11-17T23:45:07).

66 H. Fukunishi, O. Watanabe and S. Takada, On the Hamiltonian replica exchange method for efficient sampling of biomolecular systems: Application to protein structure prediction, *J. Chem. Phys.*, 2002, **116**(20), 9058–9067.

67 S. Park, T. Kim and W. Im, Transmembrane helix assembly by window exchange umbrella sampling, *Phys. Rev. Lett.*, 2012, **108**(10), 108102.

68 S. Park and W. Im, Two dimensional window exchange umbrella sampling for transmembrane helix assembly, *J. Chem. Theory Comput.*, 2013, **9**(1), 13–17.

69 M. Moradi and E. Tajkhorshid, Mechanistic picture for conformational transition of a membrane transporter at atomic resolution, *Proc. Natl. Acad. Sci. U. S. A.*, 2013, **110**(47), 18916–18921.

70 T. Okabe, M. Kawata, Y. Okamoto and M. Mikami, Replica-exchange Monte Carlo method for the isobaric–isothermal ensemble, *Chem. Phys. Lett.*, 2001, **335**(5), 435–439, DOI: **10.1016/S0009-2614(01)00055-0**.

71 G. Bussi, Hamiltonian replica exchange in GROMACS: a flexible implementation, *Mol. Phys.*, 2014, **112**(3–4), 379–384, DOI: **10.1080/00268976.2013.824126**.

72 J. Hub, B. de Groot and D. van der Spoel, g_wham-A Free Weighted Histogram Analysis Implementation Including Robust Error and Autocorrelation Estimates, *J. Chem. Theory Comput.*, 2010, **6**, 3713–3720, DOI: **10.1021/ct100494z**.

73 R. T. McGibbon, K. A. Beauchamp, M. P. Harrigan, C. Klein, J. M. Swails, C. X. Hernández, C. R. Schwantes, L.-P. Wang, T. J. Lane and V. S. Pande, MDTraj: A Modern Open Library for the Analysis of Molecular Dynamics Trajectories, *Biophys. J.*, 2015, **109**(8), 1528–1532, DOI: **10.1016/j.bpj.2015.08.015**.

74 F. Pietrucci and A. Laio, A Collective Variable for the Efficient Exploration of Protein Beta-Sheet Structures: Application to SH3 and GB1, *J. Chem. Theory Comput.*, 2009, **5**(9), 2197–2201, DOI: **10.1021/ct900202f**.

75 G. A. Tribello, M. Bonomi, D. Branduardi, C. Camilloni and G. Bussi, PLUMED 2: New feathers for an old bird, *Comput. Phys. Commun.*, 2014, **185**(2), 604–613, DOI: **10.1016/j.cpc.2013.09.018**.

76 W. Humphrey, A. Dalke and K. Schulten, VMD: visual molecular dynamics, *J. Mol. Graphics*, 1996, **14**(1), 33–38.

77 A. Panahi and C. L. Brooks III, Membrane Environment Modulates the pKa Values of Transmembrane Helices, *J. Phys. Chem. B*, 2015, **119**(13), 4601–4607, DOI: **10.1021/acs.jpcb.5b00289**.

78 A. A. Shcherbakov, P. J. Spreacker, A. J. Dregni, K. A. Henzler-Wildman and M. Hong, High-pH structure of EmrE reveals the mechanism of proton-coupled substrate transport, *Nat. Commun.*, 2022, **13**(1), 991, DOI: **10.1038/s41467-022-28556-6**.

79 I. T. Arkin and A. T. Brunger, Statistical analysis of predicted transmembrane α-helices, *Biochim. Biophys. Acta, Protein Struct. Mol. Enzymol.*, 1998, **1429**(1), 113–128, DOI: **10.1016/S0167-4838(98)00225-8**.

80 A. Senes, M. Gerstein and D. M. Engelman, Statistical analysis of amino acid patterns in transmembrane helices: the GxxxG motif occurs frequently and in association with β-branched residues at neighboring positions, *J. Mol. Biol.*, 2000, **296**(3), 921–936.

81 L. Bartoš, M. Drabinová and R. Vácha, Optimizing properties of translocation-enhancing transmembrane proteins, *Biophys. J.*, 2024, **123**(10), 1240–1252.
82 X. Wu and T. A. Rapoport, Translocation of proteins through a distorted lipid bilayer, *Trends Cell Biol.*, 2021, **31**(6), 473–484.
83 M. Hermansson and G. von Heijne, Inter-helical Hydrogen Bond Formation During Membrane Protein Integration into the ER Membrane, *J. Mol. Biol.*, 2003, **334**(4), 803–809, DOI: **10.1016/j.jmb.2003.10.019**.
84 F. Xiao Zhou, M. J. Cocco, W. P. Russ, A. T. Brunger and D. M. Engelman, Interhelical hydrogen bonding drives strong interactions in membrane proteins, *Nat. Struct. Biol.*, 2000, **7**(2), 154–160, DOI: **10.1038/72430**.
85 A. Senes, I. Ubarretxena-Belandia and D. M. Engelman, The Cα—H···O hydrogen bond: A determinant of stability and specificity in transmembrane helix interactions, *Proc. Natl. Acad. Sci. U. S. A.*, 2001, **98**(16), 9056–9061, DOI: **10.1073/pnas.161280798**.
86 J. Lee and W. Im, Role of Hydrogen Bonding and Helix −Lipid Interactions in Transmembrane Helix Association, *J. Am. Chem. Soc.*, 2008, **130**(20), 6456–6462, DOI: **10.1021/ja711239h**.
87 L. Adamian and J. Liang, Interhelical hydrogen bonds and spatial motifs in membrane proteins: polar clamps and serine zippers, *Proteins: Struct., Funct., Bioinf.*, 2002, **47**(2), 209–218.
88 C. Choma, H. Gratkowski, J. D. Lear and W. F. DeGrado, Asparagine-mediated self-association of a model transmembrane helix, *Nat. Struct. Biol.*, 2000, **7**(2), 161–166.
89 E. A. Morrison, G. T. Dekoster, S. Dutta, R. Vafabakhsh, M. W. Clarkson, A. Bahl, D. Kern, T. Ha and K. A. Henzler-Wildman, Antiparallel EmrE exports drugs by exchanging between asymmetric structures, *Nature*, 2012, **481**(7379), 45–50, DOI: **10.1038/nature10703**, (accessed 2024-01-07T10:04:12).
90 L. K. Tamm, H. Hong and B. Liang, Folding and assembly of β-barrel membrane proteins, *Biochim. Biophys. Acta, Biomembr.*, 2004, **1666**(1-2), 250–263.
91 N. Ruiz, D. Kahne and T. J. Silhavy, Advances in understanding bacterial outer-membrane biogenesis, *Nat. Rev. Microbiol.*, 2006, **4**(1), 57–66.
92 Z. Cao and J. U. Bowie, Shifting hydrogen bonds may produce flexible transmembrane helices, *Proc. Natl. Acad. Sci. U. S. A.*, 2012, **109**(21), 8121–8126, DOI: **10.1073/pnas.1201298109**, (accessed 2024/01/15).
93 N. K. Burgess, T. P. Dao, A. M. Stanley and K. G. Fleming, β-Barrel proteins that reside in the Escherichia coli outer membrane in vivo demonstrate varied folding behavior in vitro, *J. Biol. Chem.*, 2008, **283**(39), 26748–26758.
94 E. J. Danoff and K. G. Fleming, Membrane defects accelerate outer membrane β-barrel protein folding, *Biochemistry*, 2015, **54**(2), 97–99.
95 C. P. Moon and K. G. Fleming, Side-chain hydrophobicity scale derived from transmembrane protein folding into lipid bilayers, *Proc. Natl. Acad. Sci. U. S. A.*, 2011, **108**(25), 10174–10177.
96 V. Schmidt, M. Sidore, C. Bechara, J.-P. Duneau and J. N. Sturgis, The lipid environment of Escherichia coli Aquaporin Z, *Biochim. Biophys. Acta, Biomembr.*, 2019, **1861**(2), 431–440.